Chinese Journal of Natural Medicines

Highly oxygenated cembrane diterpenoids from the South China Sea soft coral *Sinularia pedunculata* and their anti-HBV activities

Ruonan Sun, Chao Huang, Zhen Gao, Ligong Yao, Yuewei Guo, Jieliang Chen, Xuwen Li

Citation: Ruonan Sun, Chao Huang, Zhen Gao, Ligong Yao, Yuewei Guo, Jieliang Chen, Xuwen Li, Highly oxygenated cembrane diterpenoids from the South China Sea soft coral *Sinularia pedunculata* and their anti-HBV activities, Chinese Journal of Natural Medicines, 2026, 24(7), 875-886. doi: 10.1016/S1875-5364(26)61191-0.

View online: https://doi.org/10.1016/S1875-5364(26)61191-0

Related articles that may interest you

Geranyl phenyl ethers from *Illicium micranthum* and their anti-HBV activity

Chinese Journal of Natural Medicines. 2022, 20(2), 139-147 https://doi.org/10.1016/S1875-5364(21)60112-7

Anti-hepatitis B virus activities of natural products and their antiviral mechanisms

Chinese Journal of Natural Medicines. 2023, 21(11), 803-811 https://doi.org/10.1016/S1875-5364(23)60505-9

Highly oxygenated clerodane furanoditerpenoids from the leaves and twigs of *Croton yunnanensis*

Chinese Journal of Natural Medicines. 2024, 22(10), 945-954 https://doi.org/10.1016/S1875-5364(24)60722-3

Dysideanones FG and dysiherbols DE, unusual sesquiterpene quinones with rearranged skeletons from the marine sponge *Dysidea avara*

Chinese Journal of Natural Medicines. 2022, 20(2), 148-154 https://doi.org/10.1016/S1875-5364(22)60161-4

Germacranolide sesquiterpenes from *Carpesium cernuum* and their anti-leukemia activity

Chinese Journal of Natural Medicines. 2021, 19(7), 528-535 https://doi.org/10.1016/S1875-5364(21)60052-3

A comprehensive review of natural products with anti-hypoxic activity

Chinese Journal of Natural Medicines. 2023, 21(7), 499-515 https://doi.org/10.1016/S1875-5364(23)60410-8

Wechat

Chinese Journal of Natural Medicines 24 (2026) 875-886

Contents lists available at ScienceDirect

Chinese Journal of Natural Medicines

journal homepage: www.cjnmcpu.com/

Original article

Highly oxygenated cembrane diterpenoids from the South China Sea soft coral *Sinularia pedunculata* and their anti-HBV activities

Ruonan Sun[a,c,Δ], Chao Huang[b,d,Δ], Zhen Gao[a,c,Δ], Ligong Yao[a,c], Yuewei Guo[a,*], Jieliang Chen[b,*], Xuwen Li[a,c,*]

[a] *Shandong Laboratory of Yantai Drug Discovery, Bohai Rim Advanced Research Institute for Drug Discovery, Yantai 264117, China*
[b] *Key Laboratory of Medical Molecular Virology (MOE/NHC), Research Unit of Cure of Chronic Hepatitis B Virus Infection (CAMS), Shanghai Frontiers Science Center of Pathogenic Microbes and Infection, School of Basic Medical Sciences, Shanghai Medical College Fudan University, Shanghai 200032, China*
[c] *State Key Laboratory of Chemical Biology, Shanghai Institute of Materia Medica, Chinese Academy of Sciences, Shanghai 201203, China*
[d] *Department of Pharmacy, Jing'an District Central Hospital of Shanghai, Shanghai 200040, China*

ARTICLE INFO

Article history:
Received 21 August 2025
Revised 8 October 2025
Accepted 16 December 2025
Available online 20 July 2026

Keywords:
Soft coral
Sinularia pedunculata
Cembrane diterpenoids
Anti-HBV activity

ABSTRACT

Eleven new highly oxygenated cembrane-type diterpenoids (**1**–**7** and **10**–**13**) and two known analogues (**8**–**9**) were isolated from the South China Sea soft coral *Sinularia pedunculata*. Their structures were determined through extensive spectroscopic analysis, quantum mechanical-nuclear magnetic resonance (QM-NMR) approach and X-ray diffraction analysis. Notably, compounds **3** and **4** were rare cembrane diterpenoids featuring a tetrahydropyran moiety with 5,8-ether and 4,8-ether linkages, respectively, while compounds **4** and **9** inhibited HBV DNA replication with IC_{50} values of 0.87 and 1.15 μmol·L^{-1} in HepAD38 cells, respectively. Mechanism investigation suggested that compound **9** accelerated capsid formation without affecting the levels of HBV cccDNA, total RNA, or pgRNA.

1. Introduction

Cembrane-type diterpenes are one of the largest and most structurally diverse class of diterpenoids [1], and most commonly found in soft corals, such as *Sinularia*, *Lobophytum*, *Sarcophyton*, and *Nephthea* [2], which possess a range of pharmacological properties, including cytotoxic [3,4], anti-inflammatory [5,6], immunomodulatory [7,8], and neuroprotective activities [9]. The soft coral genus *Sinularia* is renowned for its rich production of structurally complex and biologically potent diterpenes [10]. These compounds exhibit diverse pharmacological activities, such as cytotoxicity, anti-inflammatory effects, immunomodulation, and neuroprotection [11]. Current research categorizes the principal diterpenoids derived from *Sinularia* into 22 unique carbon skeletons [12]. This classification encompasses not only prevalent cembrane, eunicellin, and lobane systems but also multiple novel structural architectures [13]. In our ongoing exploration for cembrane diterpenoids from *Sinularia* species, previous work led to the discovery of two polyoxygenated cembranolides from *S. pedunculata*, which were shown to exert anti-inflammatory activity by suppressing NF-κB and MAPK signaling pathways, reducing inflammatory cytokine secretion, and demonstrating effective anti-inflammatory effects and colon epithelium repair in a dextran sodium sulfate (DSS)-induced acute colitis mouse model [14]. In addition, two new oxygenated cembrane diterpenes (situmulins A and B), along with nine novel cembrane-type diterpenoids (ximaonanolobatins A–I), were isolated from *S. tumulosa* and *S. nanolobata*, respectively. Notably, situmulin B showed strong antibacterial activities against fish pathogenic bacteria *S. parauberis* FP KSP28 and *P. damselae* FP2244 with minimum inhibitory concentration for 90% (MIC_{90}) values of 25 μmol·L^{-1} [15,16]. Furthermore, flexilarin D was found to have the anti-HBV activity, and the mechanism study suggested that flexilarin D could accelerate capsid formation, inhibit HBcAg, HBV core particle DNA in a dose-dependent manner [17], which motivated us to discover more cembrane diterpenoids with anti-HBV activity from soft corals *Sinularia.*

As a continuous investigation on cembrane diterpenoids with anti-HBV activity from *Sinularia* species, 11 new highly oxygenated cembrane diterpenoids (**1**–**7** and **10**–**13**) and two known ones (**8** and **9**) were isolated and elucidated by various spectral techniques and ECD calculations. Additionally, three compounds (**1**–**3**) were unambiguously confirmed by a single crystal X-ray diffraction. Among them, six compounds possessed inhibitory activity against HBV DNA replication on HepAD38 cell line *in vitro*, and compounds **4** and **9** inhibited HBV DNA replication with IC_{50} values of 0.87 and 1.15 μmol·L^{-1}, respectively. Further mechanistic studies suggested that compound **9** exerted its anti-HBV effect by reducing HBcAg levels and accelerating the capsid formation, but did not affect the levels of HBV cccDNA, total RNA, and pgRNA. Herein, details of the isolation, structural characterization, biological activity, and mechanism investigation were discussed.

2. Results and discussion

The frozen bodies of the titled animals were cut into pieces and extracted exhaustively with acetone. The Et_2O soluble por-

* Corresponding author.
E-mail addresses: ywguo@simm.ac.cn (Y. Guo); jieliangchen@fudan.edu.cn (J. Chen); xwli@simm.ac.cn (X. Li)
Δ These authors contributed equally to this work.

https://doi.org/10.1016/S1875-5364(26)61191-0
Copyright © 2026, China Pharmaceutical University. Published by Elsevier B.V. All rights are reserved.

tion of the acetone extract was repeatedly column chromatographed over silica gel, Sephadex LH-20, and RP-HPLC to yield 11 new compounds **1**–**7** and **10**–**13** (Fig. 1). Compounds **8** and **9** were readily identified as diepoxycembrene A (**8**) [18] and sinulacrassins B (**9**) [19] by comparison of their NMR data and optical rotation values with those reported in the literature, respectively.

Compound **1** was obtained as a colorless crystal. The molecular formula of **1** was established to be $C_{20}H_{32}O_3$ by positive HR-ESI-MS at *m/z* 321.2425 ([M + H]$^+$, Calcd. 321.2424) in combination with the ^{13}C NMR spectral data. The IR absorption bonds of **1** at 2964, 1644, and 980 cm^{-1} indicated the presence olefin and epoxide functionalities. The ^{1}H NMR spectrum (Table 1) of **1** displayed the presence of four methyls at δ_H 1.34 (3H, s, H_3-20), 1.32 (3H, s, H_3-18), 1.22 (3H, s, H_3-19), and 1.61 (3H, s, H_3-17), two olefinic protons at δ_H 5.71 (1H, d, *J* = 12.5Hz, H-9) and 5.78 (1H, m, H-9), two trisubstituted epoxide groups at δ_H 3.00 (1H, dd, *J* = 2.0, 7.5Hz, H-6) and δ_H 2.87 (1H, dd, *J* = 3.5, 8.5Hz, H-13). The corresponding carbons were assigned through HSQC correlations, and the ^{13}C NMR and DEPT spectroscopic data (Table 1) were in good agreement with the above analysis. The ^{1}H and ^{13}C NMR spectral data in combination with the molecular composition highly showed compound **1** to be a cembrane-type diterpene.

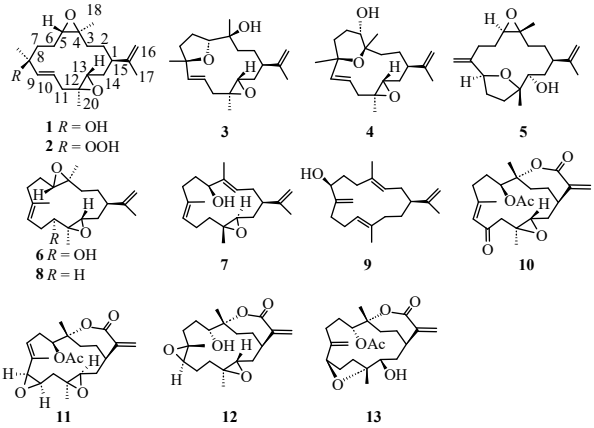


Fig. 1 The chemical structures of compounds **1**–**13**.

The planar structure and all of the assignments of ^{1}H and ^{13}C NMR data of **1** were determined by the assistance of 2D NMR studies, including ^{1}H–^{1}H COSY and HMBC experiments (Fig. 2). The ^{1}H–^{1}H COSY spectrum revealed proton sequences from H_2-3 to H_2-2/

Table 1 ^{1}H NMR (500 MHz) data of compounds **1**–**4** in $CDCl_3$.

No.	δ_H, mult. (*J*, Hz)				
	1	**2**	**3**	**4**	**5**
1	1.95 (m)	1.99 (m)	2.09 (m)	2.32 (m)	2.75 (m)
2	1.39 (m)	1.39 (m)	1.78 (m)	1.65 (m)	1.46 (m)
	1.30 (m)	1.30 (m)	1.34 (m)	1.55 (m)	1.26 (m)
3	1.68 (m)	1.68 (t, 4)	1.51 (m)	1.67 (m)	1.71 (m)
5	3.00 (dd, 7.5, 2.0)	2.94 (dd, 5, 3)	3.76 (dd, 7, 2.5)	3.54 (s)	3.32 (dd, 7.5, 3)
6	1.91 (m)	1.87 (m)	1.83 (m)	1.93 (m)	1.80 (m)
	1.42 (m)	1.52, (m)	1.66 (m)	1.76 (m)	1.61 (m)
7	1.87 (m)	1.99 (m)	1.92 (m)	1.80 (m)	2.38 (m)
	1.77 (m)	1.81 (m)	1.84 (m)	1.65 (m)	2.22 (m)
8					
9	5.71 (d, 12.5)	5.61 (d, 10)	5.74 (dd, 10, 1)	5.68 (s)	4.41 (dd, 7.5, 3.5)
10	5.78 (m)	5.72 (m)	5.83 (m)	5.66 (m)	2.08 (m)
11	2.71 (dd, 11, 3.5)	2.73 (dd, 9, 3.5)	2.68 (d, 14.5)	2.62 (dd, 14.5, 4)	2.05 (m)
	1.83 (m)	1.91 (m)	1.77 (m)	1.95	1.91 (m)
12					
13	2.87 (dd, 8.5, 3.5)	2.85 (dd, 6, 2)	2.85 (dd, 6, 3)	2.92 (dd, 9.5, 3.5)	3.65 (m)
14	1.86 (m)	1.88 (m)	2.0 (m)	2.09 (m)	1.80 (m)
	1.28 (m)	1.31 (m)	1.24 (m)	1.51 (m)	1.52 (m)
15					
16	4.74 (s)	4.76 (s)	4.72 (s)	4.79 (s)	4.78 (s)
	4.65 (s)	4.61 (s)	4.71 (s)	4.73 (s)	4.73 (s)
17	1.61 (s)	1.63 (s)	1.64 (s)	1.71 (s)	1.66 (s)
18	1.22 (s)	1.23 (s)	1.18 (s)	1.16 (s)	1.24 (s)
19	1.32 (s)	1.41 (s)	1.33 (s)	1.26 (s)	4.92 (s)
20	1.34 (s)	1.33 (s)	1.38 (s)	1.39 (s)	1.13 (s)

H-1/H_2-14/H_2-13; H-5 to H_2-6/H_2-7; H_2-5 to H-7 and H-10 to H_2-11, as shown by the bold lines in Fig. 2. Key HMBC correlations of H_3-17 to C-15, C-16 and C-1; H_3-18 to C-3, C-4 and C-5; H_3-19 to C-7, C-8 and C-9; H_3-20 to C-11, C-12 and C-13, permitted the connection of the carbon skeleton. The only hydroxyl group at C-18 was deduced by the observed HMBC correlations from H_3-19 to C-8 (δ_C 73.0). The NOE correlations of H-9 (δ_H 5.71)/H_2-11 (δ_H 2.71) suggested the double bonds $\Delta^{9,10}$ was in favor of *E* configuration (Fig. 3).

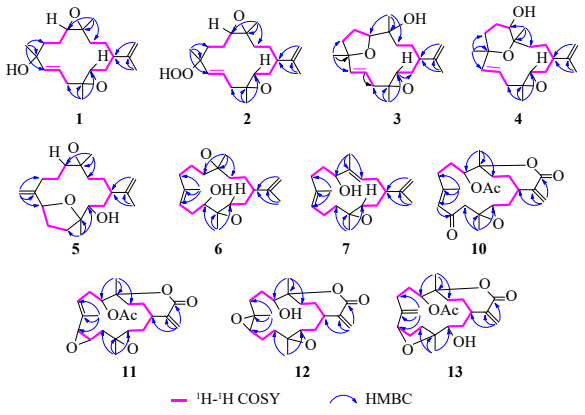


Fig. 2 Key ^{1}H–^{1}H COSY and HMBC correlations of compounds **1**–**7** and **10**–**13**.

In order to check the proposed structure as well as establish the absolute configuration of **1**, a suitable single crystal was obtained in MeOH after many attempts. A successful performance of X-ray crystallography study using Cu K_α (λ = 0.0041 Å) radiation firmly confirmed the structure of **1** and determined its absolute configuration as 1*R*,4*S*,5*S*,8*S*,11*S*,13*S* [Flack parameter: 0.02(9)] (Fig. 4, CCDC 2267364). Hence, the structure determination of **1** was completely accomplished.

Compound **2** was obtained as colorless crystal. The molecular formula of **2** was established to be $C_{20}H_{32}O_4$ by positive HR-ESI-MS at *m/z* 359.2195 ([M + Na]$^+$, Calcd. 359.2193) in combination with the ^{13}C NMR data. ^{13}C NMR and HSQC spectra (Table 2) show the presence of 20 carbons in **2**, including four methyl groups, seven methylene groups (including a terminal double bond δ_C 111.6), five methyl groups, and four quaternary carbons. A close comparison of the NMR data of compound **2** with that of the compound **1** shows that their chemical shifts are very similar, with the main difference being the chemical shifts of C-7, C-8 and C-9. The chemical shift of C-8 shifted from δ_C 84.3 in **2** to δ_C 73.0 in **1**, indicating that the hydroxyl group had become a peroxyhydroxyl group. Therefore, the plane structure of **2** is determined (Fig. 1). In order to establish the absolute configuration of **2**, a suitable single crystal was obtained from methanol after many attempts. The successful X-ray diffraction experiments with Cu Kα (λ = 0.0048 Å) radiation allowed us to confirm the proposed structure and to determine its absolute configuration as 1*R*,4*S*,5*S*,8*S*,11*S*,13*S* [Flack parameter: 0.02(14)] (Fig. 4, CCDC 2267365). Hence, the structure determination of **2** was completely accomplished.

Compound **3** was obtained as a colorless crystal and had the molecular formula $C_{20}H_{32}O_3$ on the basis of its molecular ion peak at *m/z* 321.2424 ([M + H]$^+$, Calcd. 321.2424), requiring five degrees of unsaturation. The IR absorption bands at 3442 and 1448 cm^{-1} revealed the existence of the hydroxyl and olefinic groups, which were in agreement with the presence of a terminal double bond [δ_H 4.79 (1H, s, H-16a) and 4.73 (1H, s, H-16b), δ_C 110.4 (CH_2, C-16) as indicated by the ^{1}H and ^{13}C NMR data. The ^{13}C NMR and HSQC spectra (Table 2) show the presence of 20 carbons in **3**, including four methyl groups, seven methylene groups (including a terminal double bond δ_C 110.4), five methyl groups, and four quaternary carbons. The clear HMBC correlation of H-5 (δ_H 3.76)/C-8 suggested that compound **3** forms an ether bond between C-5 and C-8. The NOE correlations of H-9 (δ_H 5.68)/H_2-11 (δ_H 1.95) suggested the double bonds $\Delta^{9,10}$ was in favor of *E* configuration. To further confirm the structure and absolute configuration of **3**, we attempted and fortunately obtained its suitable single crystals, which allowed a successful performance of X-ray crystallography study using Cu Kα radiation (λ = 0.0050 Å). Analysis of the X-ray data unambiguously confirmed the planar structure of **3** and the determination of its absolute configuration as 1*R*,4*S*,5*R*,8*S*,11*S*,13*S* [Flack parameter was 0.04(11)] (Fig. 4, CCDC 2067366). Thus, the structure of **3** was determined.

Compound **4** was also obtained as an optically active colorless oil. Its molecular formula $C_{20}H_{33}O_3$, was determined by the HR-ESI-MS molecular ion peak at *m/z* 321.2421 ([M + H]$^+$, Calcd. 321.2424). A close comparison of the NMR data of the compound **3** found that their chemical shifts were very similar, with the main difference being the chemical shifts of C-4, C-5, C-7 and C-8. The chemical shift of C-4 shifted from δ_C 72.6 in **3** to δ_C 78.2 in the low field, while the chemical shift of C-7, C-8 shifted from δ_C 38.5 to δ_C 28.7 and δ_C 80.2 to δ_C 72.6 in the high field, indicating that compound **4** formed an ether bond from C-5 and C-8. The NOE correlation between H-1 (δ_H 2.32)/H_3-18 (δ_H 1.16)/H_3-20 (δ_H 1.39)/H_2-11a (δ_H 2.62) and H-5 (δ_H 3.54)/H_3-19 (δ_H 1.26)/H_2-11b (δ_H 1.95)/H-13 (δ_H 2.92) indicate they have the same operation. Compounds **3** and **4** share the same spatial configuration, thus we infer that the absolute configuration of compound **4** is 1*R*,4*S*,5*S*,8*S*,11*S*,13*S* based on the biogenic pathway.

Compound **5** was obtained as a colorless oil. Its molecular formula was established as $C_{20}H_{32}O_3$ by HR-ESI-MS at *m/z* 321.2424 ([M + H]$^+$, Calcd. 321.2424), indicating five degrees of

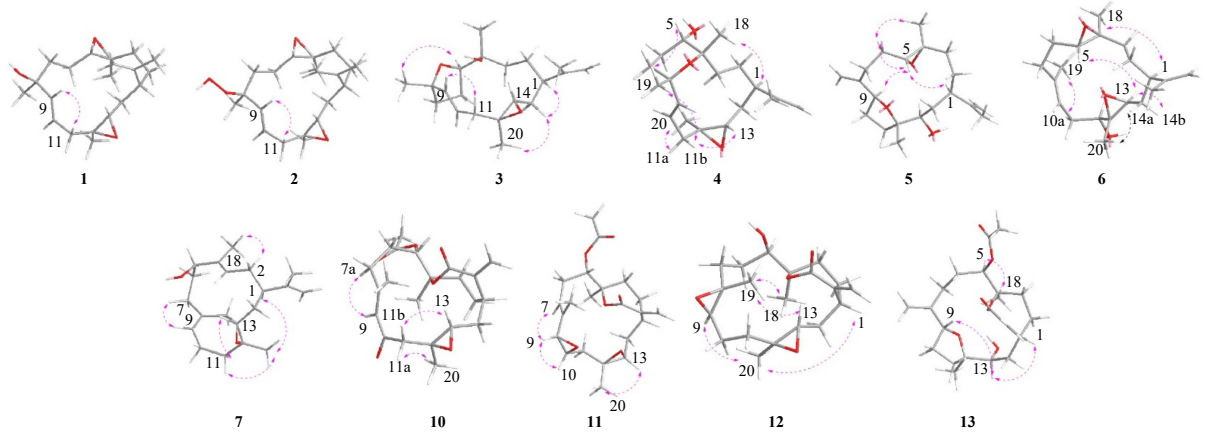


Fig. 3 Key NOESY correlations of **1**–**13**.

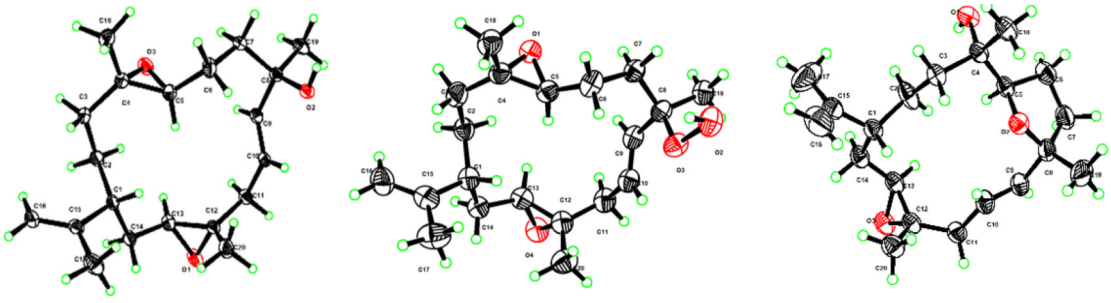


Fig. 4 The X-ray ORTEP drawings of compounds **1**–**3**.

Table 2 ^{13}C NMR data (125 MHz) of compounds **1**–**4** in $CDCl_3$.

No.	δ_c, mult.				
	1	**2**	**3**	**4**	**5**
1	44.6	44.3	47.3	43.0	41.4
2	24.7	24.8	22.8	26.9	24.8
3	31.9	32.0	39.3	37.2	32.9
4	60.8	60.7	72.6	78.2	60.8
5	60.8	60.8	79.0	68.7	60.1
6	22.3	22.6	26.1	24.1	29.4
7	37.9	34.1	38.5	28.7	31.0
8	73.0	84.3	80.2	72.6	150.8
9	140.4	135.7	140.3	140.6	80.3
10	122.1	125.5	126.4	124.7	30.8
11	43.2	42.9	41.1	41.6	38.7
12	61.2	60.8	61.2	61.6	84.9
13	62.1	61.7	61.3	61.25	73.9
14	34.5	33.9	33.8	32.5	39.4
15	147.8	147.6	147.4	148.0	149.2
16	111.5	111.6	111.0	110.37	111.5
17	18.8	19.0	18.6	21.5	19.1
18	19.8	19.6	23.3	23.2	20.1
19	31.7	24.1	28.6	31.4	111.1
20	16.5	16.8	17.3	18.7	20.9

unsaturation. The ^{13}C NMR spectrum of **5** showed 20 carbon signals, which were classified with the aid of DEPT spectrum as three methyl groups, seven sp^3 methylenes, one sp^2 methylene, four sp^3 methines (including three oxymethines), and two sp^3 quaternary and two sp^2 quaternary carbons (Tables 1 and 2). The NMR signals at δ_C 73.9 (CH) and δ_H 3.65 (1H, m) indicated the presence of a hydroperoxy group at a methine carbon. Additionally, the HSQC spectrum revealed four olefinic methylene protons at δ_H 4.93 (s), 4.90 (s), 4.78 (s), and 4.73 (s). The planar structure and assignments of ^{1}H and ^{13}C NMR data for **5** were determined through 2D NMR studies, including COSY and HMBC experiments (Fig. 2). The COSY spectrum revealed proton sequences from H_2-3 to H-13 *via* H-1, H-5 to H_2-7, and H-9 to H_2-11, as indicated by the bold lines in Fig. 2. Considering the degrees of unsaturation and ^{13}C NMR spectroscopic data, an ether linkage was placed between C-9 (δ_C 80.3) and C-12 (δ_C 84.9), and a hydroperoxy group was positioned at C-13 (δ_C 73.9). Thus, **5** was identified as a cembranoid with a 9,12-ether-linked tetrahydrofuran ring. Based on this analysis, the planar structure of **5** was established.

The relative configuration of **5** was examined by the analysis of NOE correlations, as shown in Fig. 3. In addition, the NOE correlation between H-1 (δ_H 2.75)/H_2-6a (δ_H 1.81)/H-5 (δ_H 3.32), H_3-18 (δ_H 1.24)/H_2-6b (δ_H 1.61) indicates that H-5, H_3-18 have the opposite operation. Due to lack of the NOE correlation between H-9(δ_H 4.41)/H_3-20(δ_H 1.13) indicates that they have the opposite operation. Quantum mechanical approach has become one of the most popular and reliable methods to deal with structural configuration [20, 21]. Eight possible configurations **5a** (1R^*,4R^*,5R^*,9R^*,12R^*,13R^*), **5b** (1R^*,4S^*,5S^*,9R^*,12R^*,13R^*), **5c** (1R^*,4S^*,5S^*,9S^*,12S^*,13R^*) and **5d** (1R^*,4S^*,5S^*,9S^*,12S^*,13S^*), **5e** (1R^*,4S^*,5S^*,9R^*,12R^*,13S^*), **5f** (1R^*,4R^*,5R^*,9S^*,12S^*,13S^*), **5g** (1R^*,4R^*,5S^*,9S^*,12S^*,13R^*) and **5h** (1R^*,4R^*,5R^*,9R^*,12R^*,13S^*) were applied for the calculation of the relative configuration of **5**. As a result, the experimentally observed NMR data for compound **5** gave the best match of over 93.31% possibility with the 1R^*,4R^*,5S^*,9S^*,12S^*,13R^* isomer (**5g**). Considering the presence of a single crystal of **1**–**3** and the confirmed absolute configurations at the C-1 position in the obtained compounds, we deduce that compound **5** possesses an absolute configuration of 1*R*,4*R*,5*S*,9*S*,12*S*,13*R* based on its biogenic pathway.

Compound **6** was obtained as a colorless oil. Its molecular formula was established as $C_{20}H_{32}O_3$ by HR-ESI-MS *m/z* 343.224 ([M + Na]$^+$, Calcd. 343.2244), indicating five degrees of unsaturation. The IR absorption bands at 1384, 1017, and 888 cm^{-1} indicated the presence of olefinic and epoxide functionalities. The ^{1}H NMR spectrum (Table 3) of **6** revealed four methyl groups at δ_H 1.25 (3H, s, H-20), 1.31 (3H, s, H-18), 1.83 (3H, s, H-19), and 1.64 (3H, s, H-17), one olefinic proton at δ_H 5.26 (1H, t, *J*=7.5Hz, H-8), two trisubstituted epoxide groups at δ_H 2.89 (1H, brs, H-5) and 2.92 (1H, d, *J* = 8.5 Hz, H-13). The corresponding carbons were assigned through HSQC correlations. The analysis of the ^{1}H–^{1}H COSY (Fig. 2) and HSQC spectra, in combination with ^{13}C NMR spectral data, readily facilitated the identification of three spin-spin systems [**a** (C-13 to C-1 to C-3), **b** (C-5 to C-7), and **c** (C-9 to C-11)]. Furthermore, a series of significant HMBC (Fig. 2) correlations between H_2-3, H-5 (δ_H 2.89), and H_3-18 (δ_H 1.27)/C-4; H_2-7, H-9 (δ_H 5.26), and H_3-19 [(δ_H 1.83)/C-8; H_2-11, H-13 (δ_H 2.92)], and H_3-20 (δ_H 1.31)/C-12 suggested that the partial structures **a**–**c** was connected to each other to form a 14-membered ring through the quaternary carbons C-4, C-8, and C-12. The connectivity between C-1 (δ_H 43.2) to C-15 (δ_C 147.1) was established through the HMBC cross-peaks of H_2-16/C-1, C-15, and C-17, as well as H_3-17/C-1 and C-15. Thus, the gross structure of **6** was established as depicted in Fig. 1.

The relative configuration of compound **6** was determined through NOE experiments. Clear NOE correlations were observed between H_3-19 (δ_H 1.83)/H_2-10 (δ_H 4.92) (Fig. 3), indicating the "8*E*" geometry. The clear NOE correlations between H-1 (δ_H 1.98)/H_3-18 (δ_H 1.25)/H_2-14a (δ_H 1.29)/H_3-20 (δ_H 1.31),

Table 3 ^{1}H NMR data and ^{13}C NMR data (500 MHz) of **6** and **7** in $CDCl_3$.

No.	6		7	
	δ_H, mult. (*J*, Hz)	δ_C, (mult)	δ_H, mult. (*J*, Hz)	δ_C, (mult)
1	1.98 (m)	43.2	1.92 (m)	45.9
2	1.41 (m)	25.9	2.66 (m)	29.3
	1.36 (m)		1.28 (m)	
3	1.66 (m)	32.5	5.39 (m)	127.6
	1.55 (m)			
4		60.1		137.1
5	2.89 (br s)	60.3	4.64 (t, 4.5)	67.1
6	1.99 (m)	24.4	1.89 (m)	30.4
	1.59 (m)		1.69 (m)	
7	2.39 (m)	36.2	2.20 (m)	34.0
	2.20 (m)		1.90 (m)	
8		144.5		135.1
9	5.26 (d, 7.5)	123.1	5.17 (t, 4.5)	122.9
10	4.82 (t, 7.5)	78.7	2.22 (m)	24.3
11	2.47 (d, 11)	41.7	2.12 (m)	38.4
	1.51 (m)		1.27 (m)	
12		59.2		60.3
13	2.92 (d, 8.5)	62.5	2.89 (dd, 6, 2)	62.7
14	1.88 (m)	33.4	1.83 (m)	33.8
	1.29 (m)		1.35 (m)	
15		147.1		147.3
16	4.78 (s)	111.4	4.78 (s)	110.9
	4.60 (s)		4.70 (s)	
17	1.64 (s)	19.6	1.71 (s)	19.5
18	1.25 (s)	18.9	1.71 (s)	17.2
19	1.83 (s)	17.6	1.68 (s)	17.1
20	1.31 (s)	17.8	1.30 (s)	16.5

H_3-20 (δ_H 1.31)/H-11 (δ_H 4.82) and H-5 (δ_H 2.89)/H-13 (δ_H 2.92) / H_2-14b (δ_H 1.88) indicated H-1, H-11, H_2-14a, H_3-18 and H_3-20 have the same orientations, H-5, H-13 and H_2-14b have the same orientations. On the basis of above evidence, the structure of **6** was established as 1R^*,4S^*,5S^*,11S^*,12S^*,13S^*. Due to the confirmed absolute configurations at the C-1 position in the obtained compounds, the absolute configuration of 6 was deduced as 1*R*,4*S*,5*S*,11*S*,12*S*,13*S* based on its biogenic pathway.

Compound **7** was found to possess the molecular formula $C_{20}H_{32}O_3$ as revealed by the HR-ESI-MS *m/z* 305.2479 ([M + H]$^+$, Calcd. 305.2475) and NMR data (Table 3). The IR showed absorptions band at 3440 and 1645 cm^{-1}. The presence of seven carbon signals at δ 147.3, 137.1, 135.1, 127.6, 122.9, and 110.9 and the four proton signals at δ 5.39 (1H, m), δ 5.17 (1H, t, *J* = 4.5 Hz), δ 4.78 (1H, s) and δ 4.70 (1H, s), were attributable to one terminal methylene group, and two trisubstituted double bonds. Moreover, a trisubstituted epoxide was found from the NMR signals at δ_C 62.7 (CH), 60.3 (CH_2), and δ_H 2.89 (1H, dd, *J* = 6, 2 Hz). The ^{1}H NMR spectrum also displayed signals of four methyls, including three olefinic methyl groups (δ_H 1.68, 1.70 and 1.70 each s), one methyl attached to oxycarbon (δ_H 1.30, s), and showed the signal of a hydroxy-containing methine (δ_H 4.64, d, *J* = 4.5 Hz). The planar structure of compound **7** was established through the analysis of ^{1}H–^{1}H COSY correlations and HMBC correlations.

The relative configuration of **7** was further elucidated by NOESY spectrum and QM-NMR technology by using the DP4 + protocol [22, 23]. The *E* geometry of the double bonds at C-3 and C-8 was evidenced by the presence of NOE correlations between H_2-7 and H-9 and between H_2-2 and H_3-18 (Fig. 3). The NOE correlation between H-1 (δ_H 1.92)/H_2-11a (δ_H 2.12)/H_3-20 (δ_H 1.30), H-13 (δ_H 2.89)/H_2-11b (δ_H 1.27) indicates that H-13, H_3-20 have the opposite operation. Four possible diastereoisomers (1R^*,5R^*,13R^*,14R^*)-**7a**, (1R^*,5S^*,13S^*,14S^*)-**7b**, (1R^*,5S^*,13R^*,14R^*)-**7c**, and (1R^*,5R^*,13S^*,14S^*)-**7d** were subjected to QM-NMR calculations. As a result, the experimental NMR data of compound **7** gave the best match to **7c**, with 100% probability. Consequently, the relative configuration of compound **7** could be assigned 1R^*,5S^*,13R^*,14R^*. We deduce that compound **7** possesses an absolute configuration of 1*R*,5*S*,13*R*,14*R* based on its biogenic pathway.

Compound **10** was obtained as an optically active colorless oil. The molecular formula of **10** was established to be $C_{22}H_{30}O_6$ based on HR-ESI-MS data showing a molecular ion peak at *m/z* 391.2117 ([M + H]$^+$, Calcd. for $C_{22}H_{31}O_6$, 391.2115), indicating an index of hydrogen deficiency of seven. The ^{13}C NMR data revealed the presence of 22 carbons, including seven carbons of double bonds (δ_C 124.0, 125.4, 143.3, 159.3, 168.4, 171.4, 196.7), suggesting one trisubstituted double bond and one terminal double bond. Additionally, low-field signals at δ_C 169.7 and 196.7 indicated the presence of ester and carbonyl groups. These accounted for four degrees of unsaturation, indicating that **10** has a tricyclic structure. Furthermore, analysis of ^{1}H NMR, ^{13}C NMR, DEPT, and HSQC spectra indicated the presence of 4 methyl groups (δ_C 19.4, 20.7, 21.1, 23.9), 7 methylene groups (δ_C 27.2, 29.5, 32.5, 33.1, 36.2, 53.8, 125.4), and 4 methine groups (δ_C 34.0, 60.0, 71.3, 124.0). The planar structure of **10** was further confirmed by HMBC and ^{1}H–^{1}H COSY spectra (Fig. 2). In the ^{1}H–^{1}H COSY spectrum, proton sequences from H-13 (δ_H 2.97)/H_2-14 (δ_H 2.12, 1.46) /H-1 (δ_H 3.02)/H_2-2 (δ_H 1.98, 1.30)/ H_2-3 (δ_H 2.00, 1.88), and from H-5 (δ_H 5.72)/H_2-6 (δ_H 1.79, 1.57)/H_2-7 (δ_H 2.29, 2.07) revealed two fragments (Fig. 2). The HMBC correlations from the terminal olefin H_2-16 (δ_H 6.30, 5.49) to C-1 (δ_C 34.0)/C-15 (δ_C 143.3)/C-16 (δ_C 168.4), from H_3-18 (δ_H 1.39) to C-3 (δ_C 32.5)/C-4 (δ_C 86.3)/C-5 (δ_C 71.2), H_3-19 (δ_H 2.20) to C-7 (δ_C 36.2)/C-8 (δ_C 159.3)/C-9 (δ_C 124.0), from H_3-20 (δ_H 1.54) to C-11 (δ_C 53.8)/C-12 (δ_C 58.0)/C-13 (δ_C 60.0), and from H-9 (δ_H 6.31) to C-10 (δ_C 196.7) allowed the connection of these fragments, confirming the planar structure of **10** as shown in Fig. 1.

The NOE correlations of H-7/H-9 in the NOESY spectrum suggested that the double bond $\Delta^{8,9}$ had the *E* configuration. Careful analysis of compound **10**'s NOESY spectrum reveals two key correlations: H-20 (δ_H 1.54)/H-11a (δ_H 2.99) and H-13 (δ_H2.97)/H-11b (δ_H 2.53). These observations collectively demonstrate that H-13 and H-20 occupy opposite orientations relative to the molecular plane. Further elucidation of the relative configuration of **10** was achieved using QM-NMR techniques. QM-NMR calculations were performed for four possible diastereomers: (1R^*,4R^*,5R^*,12R^*,13R^*)-**10a**, (1R^*,4R^*,5R*,12S^*,13S^*)-**10b**, (1R^*,4R^*,5S^*,12R^*,13R^*)-**10c**, and (1R^*,4R^*,5S^*,12S^*,13S^*)-**10d**.

The experimental NMR data of **10** showed the best match with **10d**, with a probability of 100%. Therefore, the relative configuration of **10** was determined to be 1R^*,4R^*,5S^*,12S^*,13S^*. Finally, the absolute configuration of **10** was determined by TDDFT-ECD calculations due to the presence of a strong chromophore near the chiral centers C-1 and C-4, revealing the absolute configuration of **10** to be 1*R*,4*R*,5*S*,12*S*,13*S* (Fig. 5).

Compound **11** was obtained as an optically active colorless

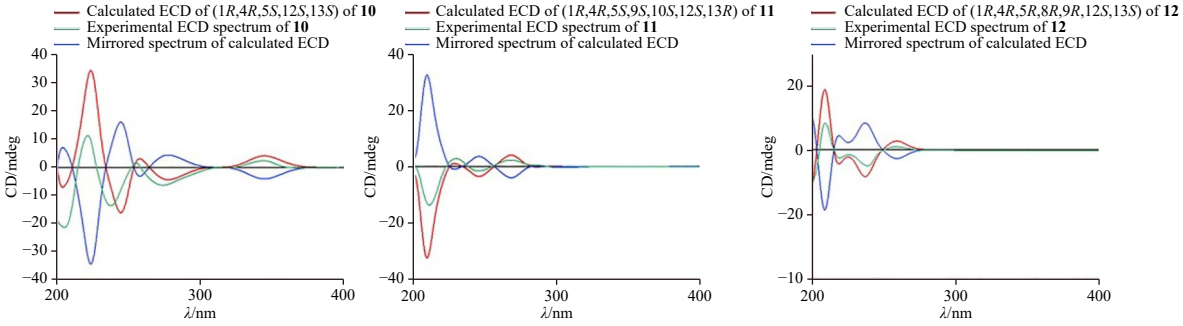


Fig. 5 TDDFT-ECD calculation and experimental ECD spectra of compounds **10**–**12**.

oil. The molecular formula of **11** was established to be $C_{22}H_{30}O_6$ based on HR-ESI-MS data showing a molecular ion peak $[M + H]^+$ at *m/z* 390.2042 (Calcd. for $C_{22}H_{31}O_6$, 390.1975), indicating an index of hydrogen deficiency of eight. The ^{13}C NMR spectrum displayed 22 carbon signals, including four methyls (δ_C 16.4, 17.8, 20.9, and 24.3), four sp^3 methylene groups (δ_C 27.4, 32.1, 32.5, and 42.1), five sp^3 methine groups (δ_C 34.5, 53.2, 54.2, 63.98, and 75.15), two oxygenated sp^3 quaternary carbons (δ_C 58.2 and 86.4), one sp^2 methylene group (δ_C 124.8), one sp^2 methine group (δ_C 125.6), and four sp^2 quaternary carbons (δ_C 135.8, 142.6, and two ester carbonyl carbons at δ_C 168.2 and 170.7). The presence of two double bonds and two ester groups accounted for four degrees of unsaturation, leaving a tricyclic structure to satisfy the remaining three degrees of unsaturation. Clear ^1H–^1H COSY correlations (Fig. 2) between H_2-3 (δ_H 2.07, 1.07)/H_2-2 (δ_H 1.50)/H-1 (δ_H 3.08)/H_2-14 (δ_H 2.22)/H-13 (δ_H 2.92), H-5 (δ_H 5.67)/H_2-6 (δ_H 2.51, 2.18)/H-7 (δ_H 5.57), and H-9 (δ_H 3.56)/H-10 (δ_H 3.11)/H_2-11 (δ_H 2.94, 0.98) indicated three spin systems. These were further connected into a 14-membered macrolide cembrane-type diterpene skeleton through HMBC correlations from H_2-16 (δ_H 6.34, 5.56) to C-15 (δ_C 142.6)/C-1 (δ_C 34.5)/C-17 (δ_C 168.2), from H_3-18 (δ_H 1.45) to C-3 (δ_C 32.5)/C-4 (δ_C 86.4)/C-5 (δ_C 75.2), from H_3-19 (δ_H 1.53) to C-7 (δ_C 124.8)/C-8 (δ_C 135.8)/C-9 (δ_C 54.2), and from H_3-20 (δ_H 1.48) to C-11 (δ_C 42.1)/C-12 (δ_C 58.2)/C-13 (δ_C 64.0). The ester bond at C-17 was linked to C-4, forming a seven-membered lactone ring. Thus, the planar structure of compound **11** was established.

In the NOESY spectrum, the NOE correlations between H-7/H-9 indicated that the $\Delta^{8,9}$ double bond has the *E* configuration. Additionally, NOE correlations between H-9 (δ_H 3.56)/H-10(δ_H 3.11) and H_3-20 (δ_H 1.48)/H-13 (δ_H 2.92) suggested that these protons have the same spatial orientation. The relative configuration of compound **11** was also determined using DP4 + probability analysis. Calculations were performed for eight possible configurations, and the results showed that the experimental NMR data of **11** closely matched the configuration $1R^*$,$4R^*$,$5S^*$,$9S^*$,$10S^*$,$12S^*$,$13R^*$, with a DP4 + probability of 100%, confirming the relative configuration of the compound. The absolute configuration of **11** was further determined by the TDDFT-ECD calculations mentioned above, resulting in an absolute configuration of 1*R*,4*R*,5*S*,9*S*,10*S*,12*S*,13*R* (Fig. 1).

Compound **12** was obtained as an optically active colorless oil. The molecular formula of **12** was established to be $C_{20}H_{30}O_5$ based on HR-ESI-MS data showing a molecular ion peak $[M + H]^+$ at *m/z* 351.2165 (Calcd. for $C_{20}H_{31}O_5$, 351.2166), indicating an index of hydrogen deficiency of six. The ^{13}C NMR spectrum displayed 20 carbon signals, including three methyls (δ_C 15.6, 20.3, and 23.0), seven sp^3 methylene groups (δ_C 24.1, 24.3, 28.4, 29.9, 32.7, 33.2, and 35.3), four sp^3 methine groups (δ_C 35.6, 58.3, 62.5, and 74.0), three oxygenated sp^3 quaternary carbons (δ_C 60.6, 59.3, and 91.0), one sp^2 methylene group (δ_C 125.4), and two sp^2 quaternary carbons (δ_C 143.4, and an ester carbonyl carbon at δ_C 168.7). The presence of one double bond, two oxirane rings, and one ester group accounted for four degrees of unsaturation, leaving a bicyclic structure to satisfy the remaining two degrees of unsaturation. Clear ^1H–^1H COSY correlations (Fig. 2) between H_2-3 (δ_H 2.05, 1.91)/H_2-2 (δ_H 2.32, 1.39)/H-1 (δ_H 2.57)/H_2-14 (δ_H 2.20, 1.47)/H-13 (δ_H 3.08), H-5 (δ_H 4.05)/H_2-6 (δ_H 1.53, 1.29)/H-7 (δ_H 1.89), and H-9 (δ_H 2.93)/H_2-10 (δ_H 1.98)/H_2-11 (δ_H 2.18, 1.39) indicated three spin systems. These were further connected into a 14-membered macrolide cembrane-type diterpene skeleton through HMBC correlations from H_2-16 (δ_H 6.29, 5.54) to C-15 (δ_C 143.4)/C-1 (δ_C 35.6)/C-17 (δ_C 168.7), from H_3-18 (δ_H 1.34) to C-3 (δ_C 32.7)/C-4 (δ_C 91.0)/C-5 (δ_C 74.0), from H_3-19 (δ_H 1.32) to C-7 (δ_C 28.4)/C-8 (δ_C 60.6)/C-9 (δ_C 58.3), and from H_3-20 (δ_H 1.31) to C-11 (δ_C 35.3)/C-12 (δ_C 59.3)/C-13 (δ_C 62.5). The ester bond at C-17 was linked to C-4, forming a seven-membered lactone ring. Therefore, the planar structure of compound **12** was established.

Compound **12** has seven chiral centers (C-1, C-4, C-5, C-8, C-9, C-12, and C-13). Due to lack of the NOE correlations between H-9 (δ_H 2.93)/H-19 (δ_H 1.32) and H_3-20 (δ_H 1.31)/H-13 (δ_H 3.08) suggested that these protons have the opposite spatial orientation. Additionally, QM-NMR calculations were applied to determine the overall relative configuration of compound **12**. Calculations and analysis of eight possible configurations showed that the experimental NMR data of **12** closely matched the configuration $1R^*$,$4R^*$,$5R^*$,$8R^*$,$9R^*$,$12S^*$,$13S^*$, with a high matching degree (98.78%). The absolute configuration of **12** was determined through TDDFT-ECD calculations. As shown in Fig. 1, the calculated Boltzmann-weighted ECD spectrum of (1*R*,4*R*,5*R*,8*R*,9*R*,12*S*,13*S*)-**12** matched well with the experimental ECD spectrum of **12**, thus establishing the absolute configuration as 1*R*,4*R*,5*R*,8*R*,9*R*,12*S*,13*S*.

Compound **13** was obtained as an optically active colorless oil. Its molecular formula, $C_{22}H_{32}O_6$, was determined by HR-ESI-MS with a molecular ion peak $[M + Na]^+$ at *m/z* 415.2084 (Calcd. for $C_{22}H_{32}O_6Na$, 415.2091), indicating seven degrees of unsaturation. The ^{13}C NMR, DEPT, and HSQC spectra revealed 22 carbon signals, including three methyl groups, nine methylene groups, four methine groups, four quaternary carbons, and two ester carbonyls (δ_C 169.5, 169.1). The two double bonds and two ester carbonyls accounted for four degrees of unsaturation, suggesting that compound **13** has a tricyclic structure. The ^1H–^1H COSY spectrum displayed cross-peaks between H_2-3/H_2-2/H-1/H_2-14/H-13, H-5/H_2-6/H_2-7, and H-9/H_2-10/H_2-11, revealing three spin systems (a–c, Fig. 2). These fragments were connected to form a cembrane skeleton by HMBC correlations from H_3-18 to C-3/C-4/C-5, from H_2-19 to C-7/C-8/C-9, and from H_3-20 to C-11/C-12/C-13. Considering one more degree of unsaturation, it was inferred that there is an epoxide ring between C-9 and C-12, a seven-membered lactone ring between C-17 and C-4, a terminal double bond at C-8 and C-19, a hydroxyl group at C-13, and an epoxy bridge between C-12 and C-13.

The relative configuration of compound **13** was mainly determined by NOE analysis and QM-NMR calculations. Due to lack

of the NOE analysis revealed the absence of correlations between H-1 (δ_H 3.41)/H_3-18 (δ_H 1.36) and H-9 (δ_H 4.25)/H_3-20 (δ_H 1.17), suggesting these protons have opposite spatial orientations. Subsequently, QM-NMR calculations further confirmed the relative configuration of compound **13** as 1*R**,4*R**,5*R**,8*R**,12*R**. Compound **13** shares the same seven-membered lactone ring fragment with other new compounds. Literature indicates that many cembrane-type diterpenes from the genus *Sinularia* possess similar structures with consistent stereochemistry at C-1 and C-4. Therefore, the absolute configurations at C-1 and C-4 in compound **13** were deduced to be the same, leading to the biosynthetic pathway that the absolute configuration of compound **13** is 1*R*,4*R*,5*R*,8*R*,12*R*.

The isolation of eleven new highly oxygenated cembrane-type diterpenoids (**1**–**7**, **10**–**13**) alongside two known analogues (**8** and **9**) from *S. pedunculata* significantly enriches the chemical diversity of marine-derived natural products (Tables 4 and 5). The structural elucidation, bolstered by QM-NMR calculations and X-ray diffraction, unequivocally confirmed the presence of rare architectural features. Notably, compounds **3** and **4** represent unusual cembrane scaffolds incorporating tetrahydropyran moieties with 5,8- and 4,8-ether linkages, respectively. Such structural motifs are scarce in natural cembranoids and may influence both the stability and bioactivity of these molecules.

Table 4 ^{1}H NMR (500 MHz) data of compounds **10**–**13** in $CDCl_3$.

No.	δ_H, mult. (*J*, Hz)			
	10	**11**	**12**	**13**
1	3.02 (m)	3.08 (m)	2.57 (m)	3.41 (m)
2	1.98 (m)	1.50 (m)	2.32 (m)	2.53 (m)
	1.30 (m)		1.39 (m)	1.09 (m)
3	2.00 (m)	2.07 (m)	2.05 (m)	1.98 (m)
	1.88 (m)	1.97 (dd, 10.5, 3)	1.91 (m)	1.86 (m)
5	5.72 (d, 7.8)	5.67 (dd, 8, 2)	4.05 (d, 12)	6.12 (d, 7. 5)
6	1.79 (m)	2.51 (m)	1.53 (m)	1.85 (m)
	1.57 (m)	2.18 (m)	1.29 (m)	1.65 (m)
7	2.29 (dd, 10.8, 4.8)	5.57(t, 5)	1.89 (m)	2.37 (m)
	2.07 (m)			2.28 (m)
9	6.31 (m)	3.56 (d, 1.5)	2.93 (d, 10.8)	4.25 (dd, 6.5, 2.5)
10		3.11 (m)	1.98 (m)	2.13 (m)
				1.93 (m)
11	2.99 (m)	2.94 (m)	2.18 (m)	2.03 (m)
	2.53 (d, 10.2)	0.98 (m)	1.39 (m)	1.91 (m)
13	2.97 (m)	2.92 (m)	3.08 (dd, 10.8, 3.6)	3.73 (dd, 7, 2.5)
14	2.12 (m)	2.22 (m)	2.20 (m)	1.80 (m)
	1.46 (m)		1.47 (m)	
16	6.30 (m)	6.34 (s)	6.29 (s)	6.25 (s)
	5.49 (m)	5.56 (m)	5.54 (s)	5.46 (s)
18	1.39 (s)	1.45 (s)	1.34 (s)	1.36 (s)
19	2.20 (s)	1.53 (s)	1.32 (s)	5.16 (s)
				4.91 (s)
20	1.54 (s)	1.48 (s)	1.31 (s)	1.17 (s)
Ac-1	2.15 (s)	2.09 (s)		2.07 (s)
OMe				3.19, s

Table 5 ^{13}C NMR data (125 MHz) of compounds **10**–**13** in $CDCl_3$.

No.	δ_C, mult. (*J*)			
	10	**11**	**12**	**13**
1	34.0	34.5	35.6	33.0
2	29.5	30.1	29.9	30.1
3	32.5	32.5	32.7	33.8
4	86.3	86.4	91.0	88.4
5	71.3	75.2	74.1	73.5
6	27.2	27.4	24.1	27.4
7	36.2	124.8	28.4	34.2
8	159.3	135.8	60.6	145.8
9	124.0	54.2	58.3	79.1
10	196.7	53.2	25.3	29.5
11	53.8	42.1	35.4	39.1
12	58.0	58.2	59.3	85.5
13	60.3	64.0	62.5	75.5
14	33.1	32.1	33.2	37.73
15	143.3	142.6	143.4	144.8
16	125.4	125.6	125.4	123.8
17	168.4	168.2	168.7	169.2
18	23.8	24.3	23.0	24.8
19	20.7	17.8	20.3	115.1
20	19.4	16.4	15.0	19.8
Ac: Me	21.1	20.9		29.5
Ac: CO	171.4	170.1		169.2
OMe				

All isolated compounds were tested for the anti-HBV activity at 4 and 20 μmol·L^{-1} in HepAD38 cells (Table S4) [24, 25]. Six compounds (**1**, **4**–**7** and **9**) showed inhibitory activity against HBV DNA replication with inhibitory ratios higher than 50% at 20 μmol·L^{-1}, compounds **4** and **9** could inhibit 60.3% and 74.3% of HBV DNA replication at 4 μmol·L^{-1}, respectively. Further analysis confirmed that compounds **4** and **9** exhibited significant anti-HBV activity with IC_{50} values of 0.87 and 1.15 μmol·L^{-1}, respectively (Fig. 6A and Table 6). Compound **9** also inhibited HBsAg and HBeAg in a dose-dependent manner (Figs. 6B and 6C) without cytotoxicity at the highest concentration (Fig. 6D), so we choose compound **9** for further investigation.

To better understand its potential, a mechanistic investigation of compound **9** was conducted. We found that compound **9** promoted capsid formation in a dose-dependent manner in HepAD38 cells (Figs. 7A and 7B). We also found that it can reduce the HBcAg level weakly only at the high dose of 100 μmol·L^{-1} (Figs. 7C and 7D), but not affect the secretion of HBsAg in HepG2-NTCP infection model (Fig. 7D). The dual-luciferase reporter assay demonstrated that compound **9** does not inhibit any of the four HBV enhancer/promoter regions (ENI/Xp, ENII/Cp, Sp1 or Sp2)

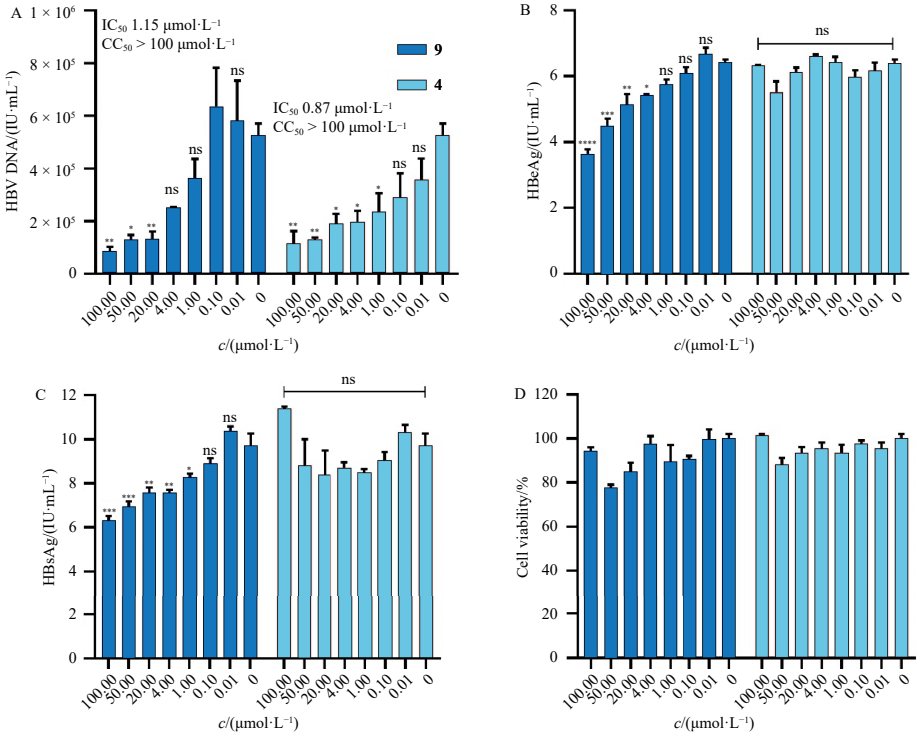


Fig. 6 The anti-HBV activity and cytotoxicity of **4** and **9** in HepAD38 cells. The Supernatant HBV DNA (A) was quantified by qPCR. The secreted HBeAg (B) and HBsAg (C) were measured by ELISA. The cell viability (D) was detected by CCK-8. Data was presented as mean ± SEM (n = 3). ns, $P > 0.05$; $^{*}P < 0.05$, $^{**}P < 0.01$, $^{***}P < 0.001$, $^{****}P < 0.0001$ *vs* the control group.

Table 6 Anti-HBV activity and cytotoxicity of compounds **4** and **9**.

Compounds	4	9	GLS4
HBV DNA IC_{50}/(μmol·L^{-1}) [a]	0.87	1.15	0.0151
HBeAg IC_{50}/(μmol·L^{-1}) [a]	> 100.00	> 100.00	6105
HBsAg IC_{50}/(μmol·L^{-1}) [a]	> 100.00	> 100.00	> 100.00
CC_{50}/(μmol·L^{-1}) [b]	> 100.00	> 100.00	> 100.00
SI [c]	> 115	> 87	> 6623

[a]: IC_{50} is the mean value for reduction of HBV DNA or HBeAg by 50% in HepAD38 cells for 3 d, Experiments were run in duplicate; [b]: CC_{50} is the mean value for cytotoxicity to HepAD38 cells for 3 d; [c]: selectivity index (SI) is the ratio of CC_{50}/HBV DNA IC_{50}; GLS4 is used as positive control.

(Fig. 8A). The results of HBV cccDNA, total RNA, and pgRNA revealed that compound **9** does not reduce their levels (Figs. 8B and 8D). The observed weak reduction in HBcAg levels (Figs. 7C and 7D) and strong promotion of capsid formation (Figs. 7A and 7B) by compound **9** is consistent with the behavior of type II core protein assembly modulator (CpAM) AB423 rather than the type I CpAM GLS4. Further docking studies have been carried out for investigation of its mechanism of action. Docking studies showed that compound **9** and **4** can both bind strongly to HBcAg (PDB ID: 5T2P). Specifically, compound **9** forming a hydrogen bond with Trp102, resulting in a docking score of −8.75, compound **4** can also form a hydrogen bond with Ser106 (Fig. 9) and the docking score is −8.96. The similar affinity of compound **9** and **4** for HBcAg may contribute to its similar anti-HBV DNA activity. Compound **9** and **4** represent promising anti-HBV candidates that warrants further investigation.

However, several aspects of this study warrant further exploration. First, *in vivo* validation of efficacy and safety in HBV-infected animal models is essential to establish the therapeutic potential of lead compounds **4** and **9**, particularly given their potent *in vitro* IC_{50} values (0.87–1.15 μmol·L^{-1}) and non-cytotoxic profiles. Second, systematic synthesis and evaluation of analogs should focus on optimizing core protein assembly modulator (CpAM) activity while addressing potential pharmacokinetic liabilities (e.g., metabolic stability, bioavailability) to enhance drug-likeness. Third, elucidating the functional consequences of accelerated capsid assembly, specifically whether it generates non-infectious or defective viral particles, is vital to understand the antiviral mechanism and clinical relevance of these type II CpAMs. Together, these studies will bridge the gap between *in vitro* promise and translational application against chronic HBV infection.

3. Experimental

3.1. General experimental procedures, animal material, extraction and isolation

For the details, please see Supporting information.

3.2. Spectroscopic data of compounds

Ximaopendunculide A (**1**): colorless crystal; $[\alpha]_D^{18}$ −39 (*c* 0.1, MeOH); IR (KBr) ν_{max} 2928, 1644, 1453, 1383, 1067, 980, 891 cm^{-1}; ^1H ($CDCl_3$, 500 MHz) and ^{13}C NMR ($CDCl_3$, 125 MHz) spectral data, see Tables 1 and 2; HR-ESI-MS: *m/z* 321.2425 $[M + H]^+$ (Calcd. for $C_{20}H_{33}O_3$, 321.2424).

Ximaopendunculide B (**2**): colorless crystal; $[\alpha]_D^{18}$ +68 (*c* 0.01, MeOH); IR (KBr) ν_{max} 2929, 1455, 1384 cm^{-1}; ^1H ($CDCl_3$, 500 MHz) and ^{13}C NMR ($CDCl_3$, 125 MHz) spectral data, see Tables 1 and 2; HR-ESI-MS: *m/z* 359.2195 $[M + Na]^+$ (Calcd. for $C_{20}H_{32}NaO_4$, 359.2193).

Ximaopendunculide C (**3**): colorless crystal; $[\alpha]_D^{18}$ −25 (*c* 0.01, MeOH); IR (KBr) ν_{max} 2927, 1448, 1383, 1052 cm^{-1}; ^1H ($CDCl_3$, 500 MHz) and ^{13}C NMR ($CDCl_3$, 125 MHz) spectral data, see Tables 1 and 2; HR-ESI-MS: *m/z* 321.2424 $[M + H]^+$ (Calcd. for $C_{20}H_{33}O_3$, 321.2424).

Ximaopendunculide D (**4**): colorless oil; $[\alpha]_D^{18}$ +230 (*c* 0.01,

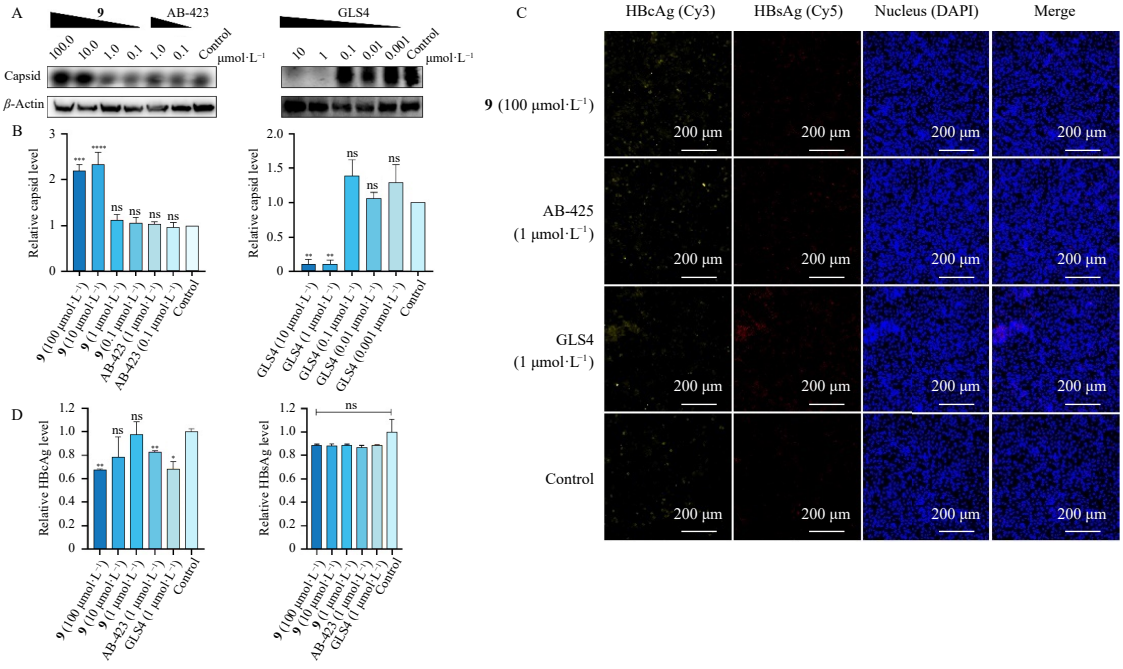


Fig. 7 The inhibitory effect of **9** on capsid and HBcAg. (A) The effect of **9** on the levels of capsid in HepAD38 cells were confirmed at the indicated concentrations **9** (0.1, 1, 10, 100 μmol·L^{-1}), AB-423 (0.1, 1 μmol·L^{-1}) and GLS4 (0.001, 0.01, 0.1, 1, 10 μmol·L^{-1}) by capsid blot at 3 day. (B) Quantification of capsid intensity. The abundance was normalized to β-actin. (C) HepG2-NTCP cells infected with HBV virions (MOI = 200) for 24 h and treated with **9** (1, 10, 100 μmol·L^{-1}), AB-423 (1 μmol·L^{-1}) and GLS4 (1 μmol·L^{-1}) immediately for 6 days. (D) the HBcAg and HBsAg intensities were analyzed by high-content fluorescence quantification. Data was presented as mean ± SEM (n = 3). ns, P > 0.05; $^{*}P$ < 0.05, $^{**}P$ < 0.01, $^{***}P$ < 0.001, $^{****}P$ < 0.0001 *vs* the control group.

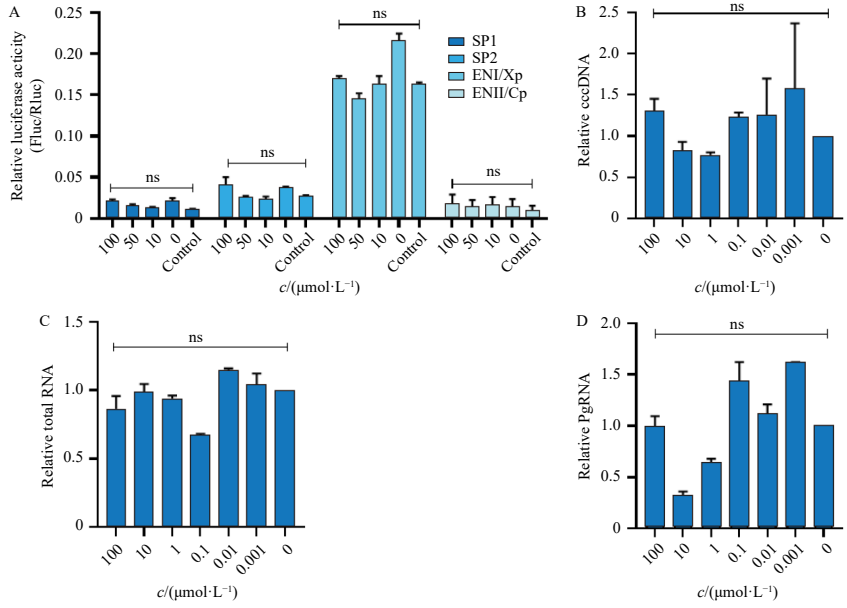


Fig. 8 Investigation of the anti-HBV mechanism of **9**. (A) Effect of **9** on the HBV promoter/enhancer. Huh7 cells transduced with four reporter plasmids (ENI/Xp, ENII/Cp, Sp1, Sp2) were treated with the indicated dose (1, 10, 50, 100 μmol·L^{-1}) for 48 h, then the cells were lysed and detected by luciferase assay. (B) The effect of **9** on the levels of cccDNA. Huh7 cells were transfected with HBVcircle (0.1 μg per well) for 8 h, then treated with the indicated concentrations of 9 (0.001, 0.01, 0.1, 1, 10,100 μmol·L^{-1}) for 3 d, cccDNA and mtDNA levels were quantified by qPCR, relative cccDNA was calculated by cccDNA/mtDNA. The effect of **9** on the levels of total HBV RNA (C) and HBV pregenomic mRNA (pgRNA) (D). HepAD38 cells were treated with the indicated concentrations of **9** (0.001, 0.01, 0.1, 1, 10,100 μmol·L^{-1}) for 5 d, RNAs were extracted for analysis of total HBV RNA and pgRNA levels by RT-qPCR. Data are presented as mean ± SEM (n = 3). ns, P > 0.05 *vs* the control group.

MeOH); IR (KBr) ν_{max} 2932, 2869, 1447, 1375, 1065, 978 cm^{-1}; ^{1}H (CDCl$_3$, 500 MHz) and ^{13}C NMR (CDCl$_3$, 125 MHz) spectral data, see Tables 1 and 2; HR-ESI-MS: m/z 321.2421 [M + H]$^{+}$ (Calcd. for $C_{20}H_{34}O_3$, 321.2424).

Ximaopendunculide E (**5**): colorless oil; $[\alpha]_D^{18}$ +53 (c 0.1, MeOH); IR (KBr) ν_{max} 2928, 2859, 1643, 1444, 1383, 1053, 905 cm^{-1}; ^{1}H (CDCl$_3$, 500 MHz) and ^{13}C NMR (CDCl3, 125 MHz) spectral data, see Tables 1 and 2; HR-ESI-MS: m/z 321.2424 [M + H]$^{+}$ (Calcd. for $C_{20}H_{33}O_3$ 321.2424).

Ximaopendunculide F (**6**): colorless oil; $[\alpha]_D^{18}$ +103 (c 0.01, MeOH); IR (KBr) ν_{max} 2926, 2857, 1384, 1017, 888 cm^{-1}; ^{1}H (CDCl$_3$, 500 MHz) and ^{13}C NMR (CDCl$_3$, 125 MHz) spectral data, see Table 3; HR-ESI-MS: m/z 343.224 [M + Na]$^{+}$ (Calcd. for $C_{20}H_{32}NaO_3$, 343.2244).

Ximaolobophytolide G (**7**): colorless oil; $[\alpha]_D^{18}$ +51 (c 0.1, MeOH); IR (KBr) ν_{max} 2923, 2857, 1645, 1447, 1384, 1050, 888 cm^{-1}; ^{1}H (CDCl$_3$, 500 MHz) and ^{13}C NMR (CDCl$_3$, 125 MHz) spectral data, see Table 3; HR-ESI-MS: m/z 305.2479 [M + H]$^{+}$ (Calcd. for $C_{20}H_{33}O_3$, 305.2475).

Ximaolobophytolide H (**10**): colorless oil; $[\alpha]_D^{18}$ +50 (c 0.01,

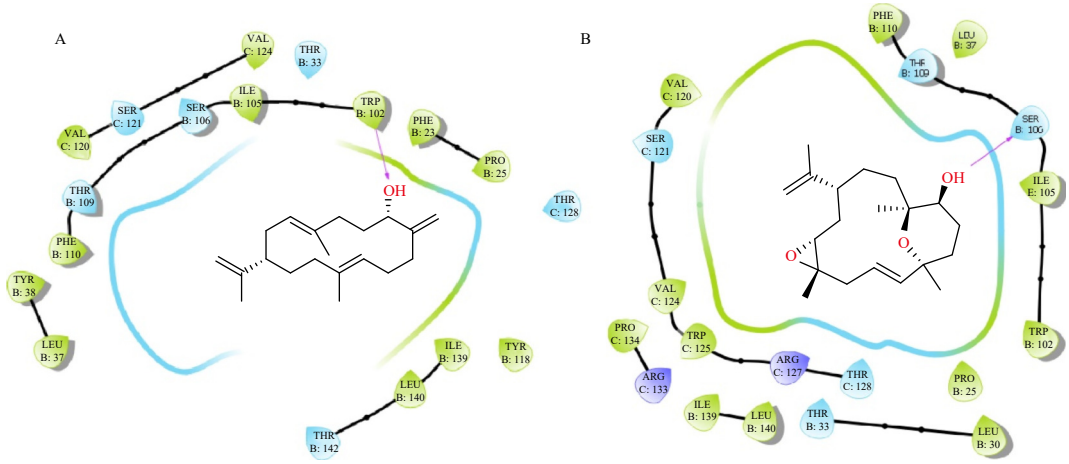


Fig. 9 The 2D protein-ligand interactions of **9** (A) and **4** (B) with 5T2P results (Purple line represent hydrogen bond).

MeOH); IR (KBr) ν_{max} 2963, 2931, 1261, 1094, 1021, 780 cm^{-1}; ^1H ($CDCl_3$, 500 MHz) and ^{13}C NMR ($CDCl_3$, 125 MHz) spectral data, see Tables 4 and 5; HR-ESI-MS *m/z* 391.2117 $[M + H]^+$ (Calcd. for $C_{22}H_{31}O_6$, 391.2115).

Ximaolobophytolide I (**11**): colorless oil; $[\alpha]_D^{18}$ +40 (*c* 0.2, MeOH); IR (KBr) ν_{max} 3444, 2935, 1739, 1711, 1384, 1233, 1140, 1043, 1019 cm^{-1}; ^1H ($CDCl_3$, 500 MHz) and ^{13}C NMR ($CDCl_3$, 125 MHz) spectral data, see Tables 4 and 5; HR-ESI-MS *m/z* 390.2042 $[M + H]^+$ (Calcd. for $C_{22}H_{30}O_6$, 390.1975).

Ximaolobophytolide J (**12**): colorless oil; $[\alpha]_D^{18}$ +270 (*c* 0.02, MeOH); IR (KBr) ν_{max} 3450, 2926, 1714, 1436, 1384, 1247, 1151, 1092 cm^{-1}; ^1H ($CDCl_3$, 500 MHz) and ^{13}C NMR ($CDCl_3$, 125 MHz) spectral data, see Tables 4 and 5; HR-ESI-MS: *m/z* 351.2165 $[M + H]^+$ (Calcd. for $C_{20}H_{31}O_5$, 351.2166).

Ximaolobophytolide K (**13**): colorless oil; $[\alpha]_D^{18}$ −20 (*c* 0.01, MeOH); IR (KBr) ν_{max} 3442, 2924, 1712, 1384, 1233, 1142, 1042 cm^{-1}; ^1H ($CDCl_3$, 500 MHz) and ^{13}C NMR ($CDCl_3$, 125 MHz) spectral data, see Tables 4 and 5; HR-ESI-MS: *m/z* 415.2084 $[M + Na]^+$ (Calcd. for $C_{22}H_{32}NaO_6$, 415.2091).

*3.3. X-ray crystallographic analysis for compounds **1–3***

The crystals of **1–3** were recrystallized from methanol at 4 °C. X-ray analyses of **1–3** were performed on a Bruker D8 Venture diffractometer with Cu Kα radiation (λ = 1.541 78 Å) at 298.0 and 150.0 K, respectively. The acquisition parameters for **1–3** are provided in the Supporting information, and crystallographic data for compounds **1** (deposition No. CCDC 2267364), **2** (deposition No. CCDC 2267365) and **3** (deposition No. CCDC 2267366) have been deposited at the Cambridge Crystallographic Data Centre. Copies of the data can be obtained free of charge *via* www.ccdc.cam.ac.uk/conts/retrieving.html.

*3.4. QM-NMR calculation of compounds **5**, **7**, and **10–13***

Conformational search employed the torsional sampling (MCMM) approach along with the OPLS_2005 force field, with a conformational search confined within an energy window of 21 $kJ{\cdot}mol^{-1}$. For conformers with populations exceeding 1% of the Boltzmann distribution, further optimization was performed at the B3LYP/6-311G (d, p) level using the IEFPCM solvent model for chloroform. Subsequently, frequency analysis was conducted to confirm that the reoptimized geometries corresponded to energy minima. Following this, NMR calculations were carried out at the PCM/mPW1PW91/6-31G (d) level, as recommended for DP4 +. NMR shielding constants were computed using the GIAO method. Finally, the shielding constants were averaged over the Boltzmann distribution for each stereoisomer and correlated with the experimental data.

3.5. In vitro anti-HBV activity and cytotoxicity

HepAD38 cells were seeded in 96-well plates at 4×10^4/well and cultured for 12 h. The control and test compounds were 100-fold diluted with medium and added into the plates with a 1% final DMSO concentration for 3 d. Cell supernatant was collected, the HBV DNA was quantified by real-time qPCR using HBV DNA detection kit (Shengxiang, Hunan, China) according to the manufacturer's protocols. Secreted HBeAg and HBsAg were measured by commercial enzyme-linked immunosorbent assay (ELISA) kits (Autobio, Zhengzhou, China) according to the manufacturer's protocols. Cell viability was detected by CCK-8 kits (Dojindo, Japan) according to the manufacturer's protocols. The concentration results in the death of 50% of the host cells (CC_{50}) of each compound. The relative effectiveness of the compound in inhibiting viral replication compared to inducing cell death was defined as the selectivity index (CC_{50} /IC_{50}).

3.6. The isolation and detection of HBV RNA

HepAD38 cells were seeded in 6-well plates at 6×10^5/well and cultured for 8 h, then cells were treated with the indicated concentrations of **9** (0.001, 0.01, 0.1, 1, 10,100 $\mu mol{\cdot}L^{-1}$) for 5 d. The isolation of cellular RNA was by TRIzol reagent and chloroform. The synthesis of cDNA was by PrimeScript RT Reagent Kit with gDNA eraser (TaKaRa, Tokyo, Japan) according to the manufacturer's protocols. RT-qPCR analysis of HBV precore /pgRNA and total RNA levels were detected by the SYBR Green qPCR Master Mix (pgRNA forward: 5′-GCCTTAGAGTCTCCTGAGCA-3′, reverse: 5′- GAGGGAGTTCTTCTTCTAGG-3′, total RNA forward: 5′-GCTTTCACTTTCTCGCCAAC-3′, reverse: 5′- GAGTTCCGCAG-TATGGATCG-3′), and were standardized to the genomic GAPDH (forward: 5′- GGTATCGTGGAAGGACTCATGAC-3′, reverse: 5′-ATGCCAGTGAGCTTCCCGTTCAGC-3′).

3.7. The detection of cccDNA in HBV circle transfection system

Huh7 cells were seeded in 48-well plates at 2×10^5/well and cultured for 8 h, cells were transfected with HBV circle (0.1 μg per well) for 12 h and treated with the indicated concentrations of **9** (0.001, 0.01, 0.1, 1, 10,100 $\mu mol{\cdot}L^{-1}$) for 3 d, the cccDNA were extracted by Qiagen miniprep columns (Cat. No. 27106), the cccDNA levels were detected by the Taqman qPCR Master Mix (cccDNA forward: 5′-CTCCCCGTCTGTGCCTTCT-3′, reverse: 5′-GCCCCAAAGCCACCCAAG-3′, probe: 5′-FAM-AGCGAAGTGCACACGGACCGGCAGA-TAM-3′), and were standardized to the mtDNA (forward: 5′-TACCGCCATCTTCAGCAAAC-3′, reverse: 5′-TAAGG-

GCTATCGTAGTTTTCTGG-3′).

3.8. Capsid blot and Western blot

HepAD38 cells were lysed with lysis buffer [1 mmol·L^{-1} EDTA, 10 mmol·L^{-1} Tris-HCl (pH 7.4), 100 mmol·L^{-1} NaCl, and 1% NP-40] on ice for 15 min, and centrifuged at 14 000 r·min^{-1} at 4 °C for 2 min. Next, samples were separated in 1.2% agarose gel by 40 V for 8 h and the HBV capsids were doblted onto a nitrocellulose membrane. Anti-HBc antibody (M-0282-0.2, Long Island, China) was used to detect the HBV capsids. The above mixtures were lysed for 15 min at 4 °C in 1oading buffer and analysed by western blot. β-Actin was used as a loading control, anti-β-actin (A1978, 1∶2000, Merk, USA).

3.9. HBV infection assay and immunofluorescence microscopy

HepG2-NTCP cells were infected with HBV virions [the multiplicity of infection (MOI) of 200] for 24 h. The cells were washed with PBS for five times, replacement of new medium containing compound **9** every 3 days for 6 days. HBcAg or HBsAg proteins were incubated with anti-HBcAg (M-0282-0.2, Long Island, China) or anti-HBsAg (M-0283-0.2, Long Island, China), which stained with Cy3 conjugated anti-rabbit antibody or Cy5 conjugated anti-mouse antibody (Thermo, MA, USA) respectively. Cell nucleus were stained with DAPI. Fluorescence was then observed and analysis using a high-content confocal microscope (Molecular Devices, ImageXpress Micro Confocal). The HBcAg or HBsAg mean intensity is expressed as the ratio of HBcAg or HBsAg intensity to nucleus intensity.

3.10. Analysis of anti-HBV mechanism by luciferase assay

Huh7 cells were seeded in 48-well plates at 2 × 10^5/well and cultured for 8 h and transfected with Fluc reporter plasmids 90 ng/well (ENI/Xp, ENII/Cp, Sp1, Sp2) and Rluc plasmids 10 ng/well for 8 h, the supernatant was replaced by new medium with the indicated dose (1, 10, 50, 100 μmol·L^{-1}) of **9**. The cells were extracted for luciferase analysis 48 h posttreatment by Dual-Luciferase Reporter Assay kits (E1910, Promega, USA) according to the manufacturer's protocols. The final result of each sample is expressed as the ratio of Fluc to Rluc.

3.11. Molecular modeling

Molecular modeling was performed by Schordinger Suite version 2021. Unless otherwise specified, default parameters were applied for all modules. The crystal structure of HBV Cp149 Y132A (PDB ID: 5T2P) was prepared using Protein Prep in Maestro. The box center was created on the cocrystallized ligand (SBA-R01), and the maximum ligand length was no more than 30 Å. Compound **9** and **4** were prepared and docked into a grid using induced-fit docking with standard precision.

4. Conclusion

In summary, 11 previously undescribed highly oxygenated cembrane-type diterpenoids and two known analogues were isolated from the South China Sea soft coral *Sinularia pedunculata*, and their structures were elucidated by UV, IR, MS, NMR spectral data, X-ray crystallographic analysis, and ECD calculations. Six compounds possessed inhibitory activity against HBV DNA replication in HepAD38 cell line *in vitro*. Importantly, compounds **4** and **9** displayed considerable anti-HBV DNA activity with the IC_{50} values of 0.87 and 1.15 μmol·L^{-1} in HepAD38, respectively. Mechanism investigation demonstrated that compound **9** reduced HBcAg levels and accelerated the formation of capsid, suggesting that it may function as a type II HBV core protein allosteric modulator. These findings expand the chemical diversity within this genus and highlight the need for further investigation into the pharmacological properties of cembrane-type diterpenoids.

Funding

This work was supported by the National Key Research and Development Program of China (No. 2021YFF0502400), the Natural Science Foundation of China (Nos. 82022069 and 42076099), Shandong Laboratory Program (No. SYS202205), the Fundamental Research Projects of Science & Technology Innovation and Development Plan in Yantai City (No. 2023JCYJ057), Taishan Scholars Program (No. tsqn202312302), the Youth Fund from Natural Science Foundation of Shandong Province (No. ZR2023QD162), the Non-profit Central Research Institute Fund of Chinese Academy of Medical Sciences (No. 2023-PT310-02), the Clinical Research Project of the Shanghai Municipal Health Commission (No. 20244Y0009), the Strategic Priority Research Program of the Chinese Academy of Sciences (No. XDB1060000), and the Key R&D Program of Shandong Province (No. 2024CXPT028).

Supplementary information

Supporting information for this study can be obtained by contacting the corresponding authors *via* E-mail.

Declaration of competing interest

These authors have no conflict of interest to declare.

References

1 Sun LL, Li WS, Li J, et al. Uncommon diterpenoids from the South China Sea soft coral *Sinularia humilis* and their stereochemistry. *J Org Chem*. 2021;86(4):3367-3376. https://doi.org/10.1021/acs.joc.0c02742.
2 Chen ZH, Lu SQ, Han GY, et al. Sinuhirtone A, an uncommon 17,19-dinorxeniaphyllanoid, and nine related new terpenoids from the Hainan soft coral *Sinularia hirta*. *Mar Drugs*. 2022;20(4):272. https://doi.org/10.3390/md20040272.
3 Kamel HN, Ding Y, Li XC, et al. Beyond polymaxenolide: cembrane-africanane terpenoids from the hybrid soft coral *Sinularia maxima* x *S. polydactyla*. *J Nat Prod*. 2009;72(5):900-905. https://doi.org/10.1021/np900040w.
4 Yang M, Li H, Zhang Q, et al. Highly diverse cembranoids from the South China Sea soft coral *Sinularia scabra* as a new class of potential immunosuppressive agents. *Bioorg Med Chem*. 2019;27(15):3469-3476. https://doi.org/10.1016/j.bmc.2019.06.030.
5 Luo ZW, Yin FC, Wang XB, et al. Progress in approved drugs from natural product resources. *Chin J Nat Med*. 2024;22(3):195-211. https://doi.org/10.1016/S1875-5364(24)60582-0.
6 Wu Q, Li XW, Li H, et al. Bioactive polyoxygenated cembranoids from a novel Hainan chemotype of the soft coral *Sinularia flexibilis*. *Bioorg Med Chem Lett*. 2019;29(2):185-188. https://doi.org/10.1016/j.bmcl.2018.12.004.
7 Lo KL, Khalil AT, Kuo YH, et al. Sinuladiterpenes A–F, new cembrane diterpenes from *Sinularia flexibilis*. *Chem Biodivers*. 2009;6(12):2227-2235. https://doi.org/10.1002/cbdv.200800298.
8 Grote D, Dahse HM, Seifert K. Furanocembranoids from the soft corals *Sinularia asterolobata* and *Litophyton arboreum*. *Chem Biodivers*. 2008;5(11):2449-2456. https://doi.org/10.1002/cbdv.200890210.
9 Su J, Yang R, Kuang Y, et al. A new cembranolide from the soft coral *Sinularia capillosa*. *J Nat Prod*. 2000;63(11):1543-1545. https://doi.org/10.1021/np0000264.
10 Xu Q, Du YQ, Chen PP, et al. Computation assisted chemical study of photo-induced late-stage skeleton transformation of marine natural products towards new scaffolds with biological functions. *Chin Chem Lett*. 2025;36(5):110141. https://doi.org/10.1016/j.cclet.2024.110141.
11 Ye F, Chen ZH, Gu YC, et al. New lobane-type diterpenoids from the Xisha soft coral *Sinularia polydactyla*. *Chin J Nat Med*. 2020;18(11):839-843. https://doi.org/10.1016/S1875-5364(20)60025-5.
12 Yan X, Liu J, Leng X, et al. Chemical diversity and biological activity of secondary metabolites from soft coral genus *Sinularia* since 2013. *Mar Drugs*. 2021;19(6):335. https://doi.org/10.3390/md19060335.
13 Wu MJ, Yu DD, Su MZ, et al. Discovery and photosynthesis of sinuaustones A and B, diterpenoids with a novel carbon scaffold isolated from soft coral *Sinularia australiensis* from Hainan. *Org Chem Front*. 2022;9(21):5921-5928.

https://doi.org/10.1039/D2QO01265K.
14 Cui YY, Jin Y, Sun RN, et al. The first discovery of marine polyoxygenated cembranolides as potential agents for the treatment of ulcerative colitis. *J Med Chem*. 2024;67(14):12248-12260. https://doi.org/10.1021/acs.jmedchem.4c00950.
15 Lin N, Li H, Wang JR, et al. New cembrane-type diterpenoids from the South China Sea soft coral *Sinularia nanolobata*. *Chin J Chem*. 2022;40(1):28-38. https://doi.org/10.1002/cjoc.202100597.
16 Xia ZY, Sun MM, Jin Y, et al. Lobosteroids A–F: six new highly oxidized steroids from the Chinese soft coral *Lobophytum* sp.. *Mar Drugs*. 2023;21(8): 457. https://doi.org/10.3390/md21080457.
17 Huang C, Jin Y, Sun RN, et al. Anti-HBV activities of cembranoids from the South China Sea soft coral *Sinularia pedunculata* and their structure activity relationship. *Chem Biodivers*. 2024;21(8): e202401146. https://doi.org/10.1002/cbdv.202401146.
18 Yamashita A, Fujimoto Y, Tamaki M, et al. Identification of antiviral agents targeting hepatitis B virus promoter from extracts of Indonesian marine organisms by a novel cell-based screening assay. *Mar Drugs*. 2015;13(11): 6759-6773. https://doi.org/10.3390/md13116759.
19 Fu PP, Jin Y, Yao LG, et al. New diterpenoids from the South China Sea soft coral *Sinularia pedunculat*a. *Tetrahedron Lett*. 2022;97:153792. https://doi.org/10.1016/j.tetlet.2022.153792.
20 Wang HR, Jin Y, Sun RN, et al. The discovery and anti-colorectal cancer activities of cembranolides from the South China Sea soft coral *Sinularia pendunculata*. *Chem Biodivers*. 2023;20(4):e202300214. https://doi.org/10.1002/cbdv.202300214.
21 Du YQ, Li H, Xu Q, et al. New cembrane-type diterpenoids with anti-inflammatory activity from the South China Sea soft coral *Sinularia* sp.. *Beilstein J Org Chem*. 2022;18:1696-1706. https://doi.org/10.3762/bjoc.18.180.
22 Zhang X, Su M, Zhu M, et al. The biologically and ecologically important natural products from the Chinese sea hare *Bursatella leachii*: structures, stereochemistry and beyond. *Chin J Nat Med*. 2024;22(11):1030-1039. https://doi.org/10.1016/S1875-5364(24)60611-4.
23 Fu A, Li Q, Xiao Y, et al. Diphenylemestrins A–E: diketopiperazine-diphenyl ether hybrids from *Aspergillus nidulans*. *Chin J Nat Med*. 2025;23(6):727-732. https://doi.org/10.1016/S1875-5364(25)60891-0.
24 Huang C, Jin Y, Fu P, et al. Discovery of novel small molecules targeting hepatitis B virus core protein from marine natural products with HiBiT-based high-throughput screening. *Acta Pharm Sin B*. 2024;14(11):4914-4933. https://doi.org/10.1016/j.apsb.2024.07.019.
25 Yang Y, Yang D, Yang Y, et al. Epigallocatechin-3-gallate suppresses hepatitis B virus replication through activating AMPK/TFEB pathway to promote autophagic degradation of viral core protein. *Chin J Nat Med*. 2026;24(3):300-312. https://doi.org/10.1016/S1875-5364(26)61105-3.